Gradual development of Γ^{5g} antiferromagnetic moment in the giant negative thermal expansion material $Mn_3Cu_{1-x}Ge_xN$ ($x \sim 0.5$)

K. Kodama,[1] S. Iikubo,[1,*] K. Takenaka,[2,3,4] M. Takigawa,[5] H. Takagi,[3,4] and S. Shamoto[1]
[1]*Quantum Beam Directorate, Japan Atomic Energy Agency, Tokai, Ibaraki 319-1195, Japan*
[2]*Department of Crystalline Materials Science, Nagoya University, Furo-cho, Chikusa-ku, Nagoya 464-8603, Japan*
[3]*RIKEN (The Institute of Physical and Chemical Research), Wako, Saitama 351-0198, Japan*
[4]*CREST, Japan Science and Technology Agency, Kawaguchi, Saitama 332-0012, Japan*
[5]*Institute for Solid State Physics, University of Tokyo, Kashiwa, Chiba 277-8581, Japan*
(Received 5 April 2010; revised manuscript received 22 May 2010; published 14 June 2010)

The antiperovskite compound $Mn_3Cu_{1-x}Ge_xN$ with $x \sim 0.5$ has a giant negative thermal expansion coefficient due to the magnetovolume effect near room temperature. Competition between the Γ^{5g} and Γ^{4g} antiferromagnetic structures around the magnetic ordering temperature could be the driving force for such a phenomenon. In order to examine this possibility, we performed neutron-diffraction experiments on $Mn_3Cu_{0.5}Ge_{0.5}N$ and ^{14}N nuclear magnetic resonance experiments on $Mn_3Cu_{0.6}Ge_{0.4}N$. As a reference material, we also investigated Mn_3NiN, whose spin structure is represented by a linear combination of the Γ^{5g} and Γ^{4g} antiferromagnetic components. We conclude that in $Mn_3Cu_{1-x}Ge_xN$ ($x \sim 0.5$), the Γ^{4g} antiferromagnetic component is nearly absent and the competition between the Γ^{5g} and Γ^{4g} antiferromagnetic structures is irrelevant to the giant negative thermal expansion coefficient. The Γ^{5g} antiferromagnetic ordered moment gradually develops with decreasing temperature. This provides a thorough justification for the analysis presented in the previous letter [S. Iikubo *et al.*, Phys. Rev. Lett. **101**, 205901 (2008)].

DOI: 10.1103/PhysRevB.81.224419 PACS number(s): 75.25.−j, 75.80.+q, 76.60.−k, 65.40.De

I. INTRODUCTION

Precise control of material volume is often required in advanced industrial applications. In electronic devices, for example, the required precision in length is on the order of nanometer. For such applications, it is essential to control the temperature (T) variation in material volume, i.e., the thermal expansion. Indeed development of materials with negative or nearly zero-thermal expansion coefficients has been an important mission of materials science. A possible mechanism for the negative or zero-thermal expansion coefficient is magnetovolume effect (MVE) or Invar effect in an itinerant electron magnet, i.e., the volume expansion caused by magnetic ordering.[1–4] However, in many materials which exhibit large MVEs, the volume expansion is very sharp against T because the ordered magnetic moment rapidly increases below the magnetic transition temperature. The volume expansion can be even discontinuous when the magnetic transition is first order, of which an example will be shown later. Then MVE must be broadened against T in order to obtain the material with the negative or zero-thermal expansion. Recently, large negative thermal expansion and zero-thermal expansion were realized by broadening MVE against T in the antiperovskite manganese nitrides.[5–8] Understanding the mechanism of the broadening of MVE in this system must give a key information to develop a new functional material with the negative or zero-thermal expansion.

In the antiperovskite manganese nitrides Mn_3AN, where A is a transition metal or semiconducting element such as Mn, Ni, Cu, Zn, Ge, Sn, and Ag, the A atoms are located in the corner positions of the cubic lattice and the Mn and N atoms are at the face- and body-centered positions, respectively.[9,10] These compounds have attracted keen interest due to a large variety of magnetic orders and structural phase transitions.[9,11–16] For some A elements (for example, A=Ga, Zn, and so on), these materials are well known for a large MVEs.[9,17–20] However, all of them with MVEs exhibit a sharp volume change against T.

The broadening of MVE in antiperovskite manganese nitrides is caused by the substitution of only Ge and Sn atoms for A site.[5–7] As a typical example, the MVE observed in the $Mn_3Cu_{1-x}Ge_xN$ system is shown in Fig. 1.[5,6] Mn_3CuN (x=0) exhibits ferromagnetic transition at T_C=143 K accompanied by a cubic to tetragonal structural phase transition.[9] The change in the linear thermal expansion $\Delta L/L$ is negligibly small across the transition. For x=0.15, a magnetic ordering takes place at $T \sim 100$ K accompanied by a large and sharp increase in $\Delta L/L$ immediately below the ordering temperature. For larger x, the ordering temperature increases and the change in $\Delta L/L$ becomes gradual, taking place over a

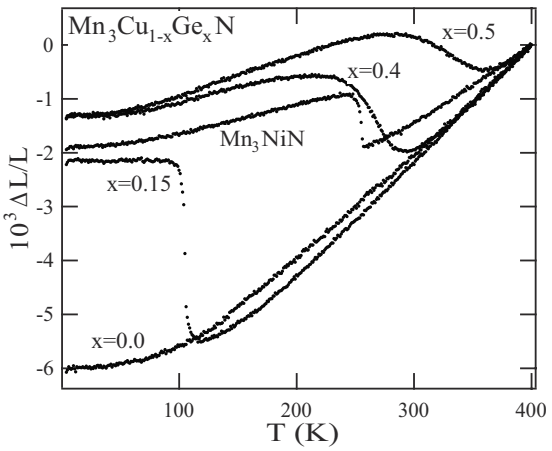

FIG. 1. Temperature dependence of linear thermal expansions of $Mn_3Cu_{1-x}Ge_xN$ (Refs. 5 and 6) and Mn_3NiN (Ref. 24).

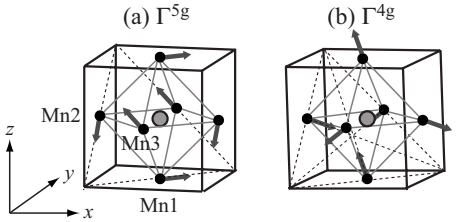

FIG. 2. (a) Γ^{5g}-type and (b) Γ^{4g}-type antiferromagnetic structures. Large and small circles show N and Mn atoms, respectively. In both magnetic structures, the angle between the nearest-neighbor Mn moments is 120° while the second nearest-neighbor moments point to the same direction.

broader T range. For $x \sim 0.5$, $\Delta L/L$ is almost linear in T in the temperature range $270 \leq T \leq 350$ K with the negative thermal expansion coefficient $\alpha \sim -2 \times 10^{-5}$. The absolute value of α is larger than the reported values for other materials with negative thermal expansion coefficients such as ZrW_2O_8 and $AlPO_4$, for which $\alpha \sim -1 \times 10^{-5}$.[21] Recent results of powder neutron diffraction have revealed that materials with large MVEs ($x \geq 0.15$) commonly have cubic crystal structures with a space group of $Pm\bar{3}m$ below the magnetic ordering temperature and the Γ^{5g}-type antiferromagnetic structure (shown later) with the ordered moment 2–2.3 μ_B at the lowest temperature.[22]

In the previous letter,[23] we discussed the mechanism of negative thermal expansion coefficients and the broadened MVE in $Mn_3Cu_{1-x}Ge_xN$. First, we argued that the volume change below the antiferromagnetic ordering temperature (T_N) correlates with the temperature dependence of the amplitude of the Γ^{5g} antiferromagnetic ordered moment. This is based on the results of neutron-diffraction and nuclear magnetic resonance (NMR) experiments showing that the Γ^{5g} amplitude gradually increases with decreasing T in those samples which show broadened MVEs, i.e., gradual increase in the volume. Second, we proposed that the local lattice distortion detected by the measurement of the atomic pair-distribution function (PDF) triggers the gradual increase in the Γ^{5g} antiferromagnetic ordered moment. However, the first point was not immediately obvious since it was deduced through detailed analyses and arguments on the results of neutron diffraction and NMR, and the details were not described in the letter.

In this paper detailed analysis and arguments are presented on the results of neutron diffraction and NMR on $Mn_3Cu_{1-x}Ge_xN$ with $x \sim 0.5$ and Mn_3NiN as a reference material. As mentioned in Ref. 22 the magnetic Bragg peak was observed at $q=(000)$. There are three possible magnetic eigenstates for this wave vector: a collinear ferromagnetic structure (not shown), and the Γ^{5g}- and Γ^{4g}-type antiferromagnetic structures shown in Figs. 2(a) and 2(b).[9] As mentioned above, the samples that exhibit large MVEs have the Γ^{5g} antiferromagnetic structure or at least do so at the lowest temperature. If the Γ^{4g} antiferromagnetic ordering do not causes MVE, the following three cases can be considered as the mechanism for the broadened MVE:

Case (1): ordered phases with Γ^{5g} and Γ^{4g} antiferromagnetic structures with ordered moments of about 2 μ_B coexist, and their volume fractions continuously change with T. Case (2): the magnetic structure of the system can be represented by a linear combination of Γ^{5g} and Γ^{4g} antiferromagnetic structures, and the weight of the Γ^{5g} component gradually increases with decreasing T. Case (3): in the whole T region the Γ^{4g} component is basically absent and Γ^{5g} antiferromagnetic ordered moment gradually increases with decreasing T.

In Sec. III A we present the results of powder neutron diffraction and ^{14}N-NMR on Mn_3NiN, whose magnetic structure is a linear combination of Γ^{5g} and Γ^{4g} antiferromagnetic structures below $T_N \sim 250$ K.[9,19] Detailed results of powder neutron diffraction on $Mn_3Cu_{0.5}Ge_{0.5}N$ ($T_N \sim 370$ K) are then reported in Sec. III B, which exclude the case (1). In Sec. III C, the results of ^{14}N-NMR on $Mn_3Cu_{0.6}Ge_{0.4}N$ ($T_N \sim 290$ K) are given to demonstrate that the case (2) can be excluded while the case (3) is a valid model.

II. EXPERIMENTS

All of the samples were prepared by solid-state reaction. Linear thermal expansion was measured using a strain gage (KYOWA; type KFL). The details were described in the previous paper.[6]

Powder neutron-diffraction measurements of $Mn_3Cu_{0.5}Ge_{0.5}N$ and Mn_3NiN were performed using the high-resolution powder diffractometer (HRPD) [neutron wavelength: 1.8228 Å, collimations: open (effective value of 35′)-20′-6′] and the triple axes spectrometer TAS-2 (neutron wavelength: 2.3590 Å, collimation: 14′-40′-40′-80′) installed in the reactor JRR-3 of JAEA. The powder samples were set in vanadium holders enclosed in Al cans filled with He gas. They were mounted in a closed-cycle refrigerator or in a furnace for measurements below or above the room temperature, respectively.

NMR measurements of ^{14}N nuclei with the nuclear spin of $I=1$ were performed using the standard spin-echo technique. The NMR spectra of Mn_3NiN were obtained by plotting the integrated intensity of the spin echo signal as a function of frequency at the fixed magnetic field of 6.615 T. The measured frequencies range from 18 to 23 MHz. For $Mn_3Cu_{0.6}Ge_{0.4}N$ the spin-echo intensity was recorded as a function of magnetic field at the fixed resonance frequency of 19.90 MHz. The measured magnetic fields range from 6.1 to 6.9 T.

III. RESULTS AND DISCUSSIONS

In Sec. I, we mentioned the possibility of coexistence of the Γ^{4g} and Γ^{5g} antiferromagnetic structures in $Mn_3Cu_{1-x}Ge_xN$ with $x \sim 0.5$. In the following, we demonstrate that the Γ^{4g} antiferromagnetic moments give a finite hyperfine field at the N site contributing to the NMR linewidth while the hyperfine field is cancelled for the Γ^{5g} antiferromagnetic moments. Therefore, NMR provides a powerful method to judge whether the magnetic structure contains a Γ^{4g} antiferromagnetic component or not.

In the antiperovskite manganese nitride with the cubic structure, the nitrogen atoms are located in the center of the Mn octahedra. In this case, the isotropic hyperfine interaction between the N nuclei and the antiferromagnetic Mn moments results in zero hyperfine field at the N nuclei. Hence only the anisotropic interaction should be considered. Among three Mn atoms shown in Fig. 2(a), let us first consider the anisotropic hyperfine interaction between the Mn1 moment and the N nuclear spin. Since the Mn1-N bond, which is parallel to the z axis, has fourfold rotational symmetry in the cubic antipervskite structure, the anisotropic part of the hyperfine tensor is represented as follows:

$$\tilde{A}_1 = \begin{pmatrix} A_\perp & 0 & 0 \\ 0 & A_\perp & 0 \\ 0 & 0 & A_\parallel \end{pmatrix},$$

where $2A_\perp + A_\parallel = 0$. Likewise the hyperfine tensors for the Mn2-N and Mn3-N bonds are represented as

$$\tilde{A}_2 = \begin{pmatrix} A_\parallel & 0 & 0 \\ 0 & A_\perp & 0 \\ 0 & 0 & A_\perp \end{pmatrix}$$

and

$$\tilde{A}_3 = \begin{pmatrix} A_\perp & 0 & 0 \\ 0 & A_\parallel & 0 \\ 0 & 0 & A_\perp \end{pmatrix},$$

respectively. The hyperfine field at N site is obtained by the following equation:

$$\boldsymbol{H}_{\rm hf} = \tilde{A}_1 \cdot \boldsymbol{M}_1 + \tilde{A}_2 \cdot \boldsymbol{M}_2 + \tilde{A}_3 \cdot \boldsymbol{M}_3, \quad (1)$$

where $\boldsymbol{M}_1$, $\boldsymbol{M}_2$, and $\boldsymbol{M}_3$ are the magnetic moments of Mn1, Mn2, and Mn3 sites, respectively. In the case of the Γ^{4g} antiferromagnetic structure, $\boldsymbol{M}_1$, $\boldsymbol{M}_2$, and $\boldsymbol{M}_3$ are given as

$$\boldsymbol{M}_1 = \sqrt{\frac{2}{3}} \begin{pmatrix} -\frac{1}{2} \\ \frac{1}{2} \\ 1 \end{pmatrix}, \quad \boldsymbol{M}_2 = \sqrt{\frac{2}{3}} \begin{pmatrix} 1 \\ \frac{1}{2} \\ -\frac{1}{2} \end{pmatrix},$$

$$\boldsymbol{M}_3 = \sqrt{\frac{2}{3}} \begin{pmatrix} -\frac{1}{2} \\ -1 \\ -\frac{1}{2} \end{pmatrix}. \quad (2)$$

Here, the magnitude of the magnetic moment is normalized to unity. By substituting Eqs. (2) into Eq. (1), the hyperfine field from the Γ^{4g} antiferromagnetic moment, $H_{\rm hf}^{\Gamma^{4g}}$, is obtained as

$$\boldsymbol{H}_{\rm hf}^{\Gamma^{4g}} = \sqrt{\frac{2}{3}}(A_\parallel - A_\perp) \begin{pmatrix} 1 \\ -1 \\ 1 \end{pmatrix}. \quad (3)$$

Thus the Γ^{4g} antiferromagnetic structure induces a finite hyperfine field parallel to the $[1\bar{1}1]$ direction. This field contributes to the width of the ^{14}N-NMR spectrum in the powder sample.

On the other hand, the Γ^{5g} antiferromagnetic structure are represented as follows:

$$\boldsymbol{M}_1 = \sqrt{\frac{1}{2}} \begin{pmatrix} 1 \\ 1 \\ 0 \end{pmatrix}, \quad \boldsymbol{M}_2 = \sqrt{\frac{1}{2}} \begin{pmatrix} 0 \\ -1 \\ -1 \end{pmatrix},$$

$$\boldsymbol{M}_3 = \sqrt{\frac{1}{2}} \begin{pmatrix} -1 \\ 0 \\ 1 \end{pmatrix}. \quad (4)$$

By substituting Eqs. (3) into Eq. (1), we get

$$\boldsymbol{H}_{\rm hf}^{\Gamma^{5g}} = 0. \quad (5)$$

The hyperfine field from the Γ^{5g} antiferromagnetic moments is perfectly cancelled out, therefore, no broadening of ^{14}N-NMR spectrum is induced. (As shown later, in the presence of local breaking of the cubic symmetry,[23] the Γ^{5g} antiferromagnetic moments do provide a finite hyperfine field at the N sites, which is much smaller than the field induced by the Γ^{4g} antiferromagnetic moments.)

A. Neutron diffraction and NMR of Mn_3NiN

First, in this section we report the results of the neutron diffraction and ^{14}N-NMR measurements in Mn_3NiN in order to estimate the width of the ^{14}N-NMR spectrum induced by the Γ^{4g} antiferromagnetic ordered moments. Mn_3NiN has a magnetic structure expressed as a linear combination of the Γ^{5g} and Γ^{4g} antiferromagnetic components below $T_N \sim 250$ K.[9,19] As shown in Fig. 1, Mn_3NiN exhibits a sharp MVE around T_N. The change in linear thermal expansion at T_N in Mn_3NiN is about 1/4 of that in $Mn_3Cu_{0.85}Ge_{0.15}N$.[24]

Figure 3 shows the neutron-scattering profile of Mn_3NiN at 10 and 300 K, measured at TAS-2 spectrometer. The ordered moments of the Γ^{5g} and Γ^{4g} components can be estimated at various temperatures using the integrated intensities of 100, 110, 111, 200, 210, and 211 Bragg reflections, as indicated in Fig. 4. Among these Bragg reflections, the 111 and 200 reflections originate solely from nuclear scattering while the other reflections have contribution from both nuclear and magnetic scatterings. The structural parameters corresponding to the cubic crystal structure with the space group of $Pm\bar{3}m$ are used in the calculation of intensities (all atoms are fixed at special positions). The amplitudes of ordered moments of the Γ^{5g} and Γ^{4g} components are refined by the least-squares fitting program. In estimating the magnetic moments the isotropic magnetic form factor of Mn^{3+} (Ref. 25) is used. The estimated ordered moments are not consistent with the values obtained by Fruchart *et al.*[19] They re-

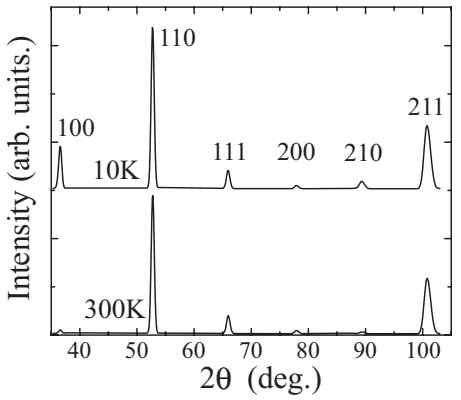

FIG. 3. Neutron-scattering profile in Mn_3NiN at 10 and 300 K. The data were collected using TAS-2.

ported that the Γ^{4g} antiferromagnetic ordered moment becomes zero at about 170 K and the Γ^{5g} ordered moment is about 1 μ_B at 77 K. The temperature dependence of the magnetization of the sample used in the present measurements also differs from their data, indicating that the magnetic behavior of this system is sample-dependent due, for example, to slight differences in the nitrogen composition.

Figure 5 shows the ^{14}N-NMR spectra at the applied field of 6.615 T and at various temperatures. At 300 K the spectrum has a two-peak structure although all the N atoms are crystallographically equivalent in the reported cubic structure. This may appear to be due to an inhomogeneity of the crystal structure in this sample caused by, for example, nitrogen deficiency. Below T_N (~250 K), broadening of the spectrum is obvious. Note that the width of the spectra decreases with decreasing T, similar to the temperature dependence of the ordered moment of the Γ^{4g} antiferromagnetic structure. In Fig. 6, the full width at half maximum (FWHM) of the ^{14}N-NMR spectrum is plotted against the amplitude of the Γ^{4g} antiferromagnetic ordered moment. Assuming that the Γ^{5g} component makes negligible contribution to the line width, the coupling constant $A_{\Gamma^{4g}}$ between the FWHM and the Γ^{4g} antiferromagnetic moment is defined as

$$\mathrm{FWHM(MHz)} = {}^{14}\gamma_N A_{\Gamma^{4g}} M_{\Gamma^{4g}}, \tag{6}$$

where $^{14}\gamma_N$ is the nuclear gyromagnetic ratio of ^{14}N (3.0756 MHz/T). The solid line in Fig. 6 gives the value of $A_{\Gamma^{4g}}$ as

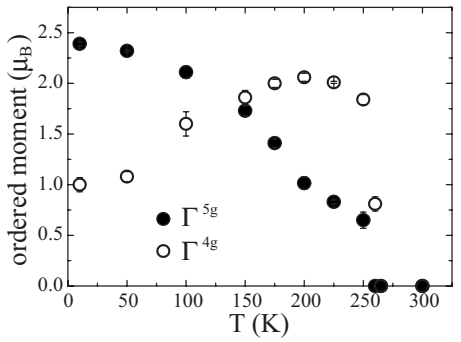

FIG. 4. Temperature dependence of Γ^{5g} and Γ^{4g} antiferromagnetic ordered moments with Mn_3NiN.

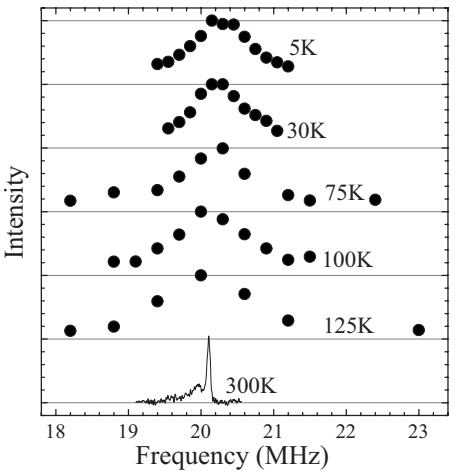

FIG. 5. NMR spectra of ^{14}N nuclei in Mn_3NiN at various temperatures. The data were collected at a fixed magnetic field of 6.615 T.

0.23 ± 0.01 T/μ_B. This value is used in the analysis of the result of ^{14}N-NMR on $Mn_3Cu_{0.6}Ge_{0.4}N$ in Sec. III C.

B. Results of neutron diffraction on $Mn_3Cu_{0.5}Ge_{0.5}N$

Figure 7 shows the neutron-diffraction patterns of $Mn_3Cu_{0.5}Ge_{0.5}N$ ($T_N \sim 400$ K) at various temperatures obtained by HRPD. In order to investigate the three cases mentioned in Sec. I, the volume fractions or the ordered moments of the Γ^{5g} and Γ^{4g} components are estimated. First, assuming the magnetic structure represented by a linear combination of the Γ^{5g} and Γ^{4g} components [case (2)], the ordered moments of both components are estimated from the integrated intensities of the six Bragg reflections shown in Fig. 7 at several temperatures. The results are shown in Fig. 8(a). Around 100 K Γ^{5g} component of the ordered moment saturates at the value 2.59 μ_B and the Γ^{4g} component is nearly zero. Second, if we consider the case (1), where the ordered phases with Γ^{5g} and Γ^{4g} antiferromagnetic structures coexist, we can roughly estimate the volume fractions of two components from the data shown in Fig. 8(a). Here we assume that the magnetic moments of the Γ^{5g} and Γ^{4g} antiferromagnetic phases are independent of T and their values are 2.59 μ_B.

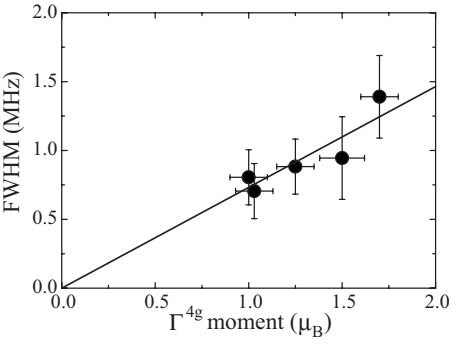

FIG. 6. FWHM of the ^{14}N-NMR spectra in Mn_3NiN is plotted against the ordered moment of Γ^{4g} antiferromagnetic structure. The solid line shows the fitting to Eq. (6).

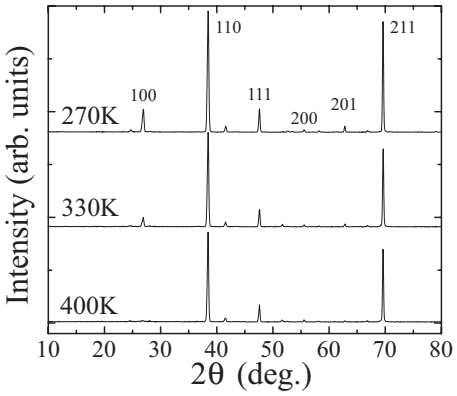

FIG. 7. Neutron-diffraction patterns of $Mn_3Cu_{0.5}Ge_{0.5}N$ at 400, 330, and 270 K. The data were collected using HRPD.

The volume fractions of the Γ^{5g} and Γ^{4g} antiferromagnetic phases, $\alpha(T)$ and $\beta(T)$ can be estimated by following equations:

$$\alpha(T) = \left[\frac{M_{\Gamma^{5g}}(T)}{2.59\ \mu_B}\right]^2, \quad \beta(T) = \left[\frac{M_{\Gamma^{4g}}(T)}{2.59\ \mu_B}\right]^2,$$

where $M_{\Gamma^{5g}}(T)$ and $M_{\Gamma^{4g}}(T)$ correspond to the data of Fig. 8(a). The estimated volume fractions are shown in Fig. 8(b). When case (1) is considered we also assumed a finite fraction

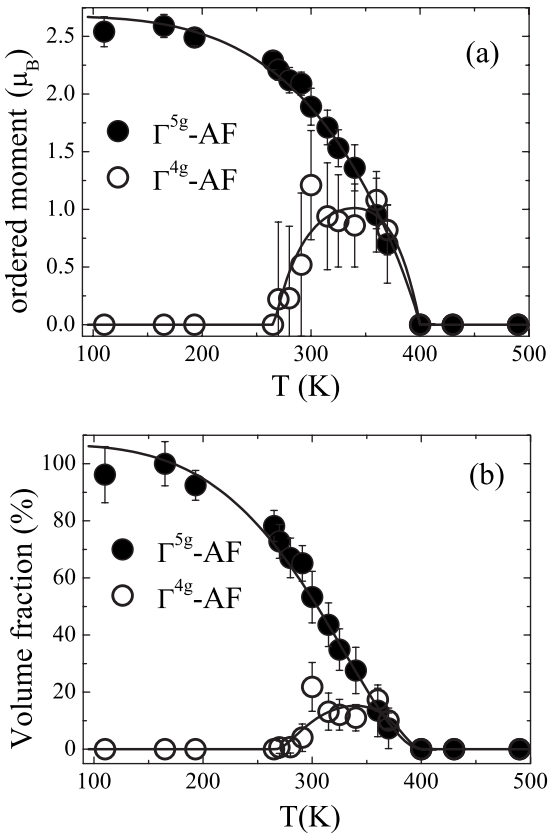

FIG. 8. (a) The ordered moments and (b) the volume fractions of Γ^{5g}- and Γ^{4g}-type antiferromagnetic structures estimated from the neutron-diffraction results on $Mn_3Cu_{0.5}Ge_{0.5}N$. Lines are guide for the eyes.

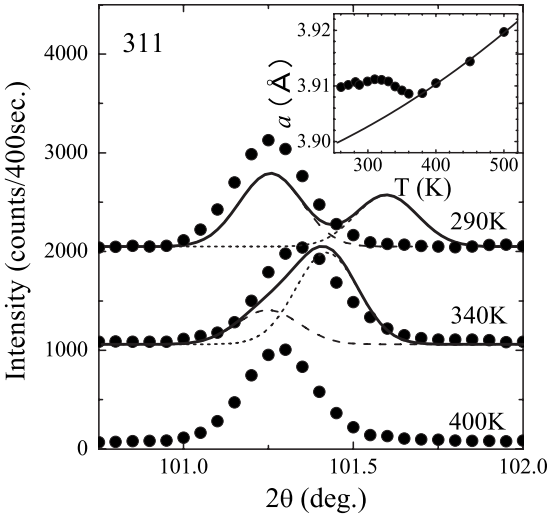

FIG. 9. Main panel: the observed (closed circles) and calculated (solid lines) profiles of 311 reflection at 290, 340, and 400 K. The dashed and fine dotted lines show the calculated profiles of the Γ^{5g} antiferromagnetic phase with a large lattice constant, and the Γ^{4g} antiferromagnetic and paramagnetic phases with small lattice constants, respectively. Details are given in the text. Inset: The lattice constant of $Mn_3Cu_{0.5}Ge_{0.5}N$ is plotted against T by closed circles. The solid line shows the fitting the data above 380 K to a quadratic function against T and an extrapolation of the fitting function to lower temperatures.

of the paramagnetic phase because the sum of the volume fractions of Γ^{5g} and Γ^{4g} component does not reach 100% in the temperature region where both phases coexist.

Let us now demonstrate that case (1) can be excluded based on the neutron-diffraction data. In case (1), it is assumed that only the Γ^{5g} antiferromagnetic phase exhibits large MVE, and the Γ^{4g} antiferromagnetic and paramagnetic phases do not exhibits MVE. The lattice constant of the Γ^{5g} antiferromagnetic phase should be larger than the lattice constants of the Γ^{4g} antiferromagnetic and paramagnetic phases. Then the Bragg peaks due to nuclear scattering should split into two in the temperature region at which these phases coexist. Specifically we looked at the 311 reflection since it has contribution only from nuclear scattering.[22] Fig. 9 shows the calculated (solid lines) and the observed (closed circles) profiles of the 311 reflection. The calculated profile is the sum of contributions from the Γ^{5g} antiferromagnetic phase, and Γ^{4g} antiferromagnetic and the paramagnetic phases represented by the dashed and dotted lines, respectively. The peak profiles of the Γ^{5g} antiferromagnetic phase at 290 and 340 K were calculated using the experimental lattice constants at 290 and 340 K. On the other hand, the profiles of the Γ^{4g} antiferromagnetic and paramagnetic phases 290 and 340 K were calculated by extrapolating the lattice constant observed above 380 K given in Ref. 22 down to lower temperatures. We also took into account the instrumental resolution represented by a Gaussian with the FWHM of 0.22 degrees, which is obtained from the diffraction data on Si powder in the same collimations. Obviously, the calculated profiles below T_N is not compatible with the experimental data, excluding the possibility of case (1).

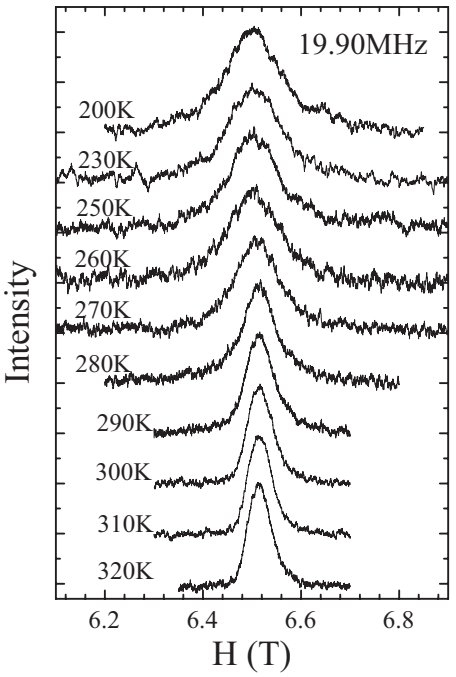

FIG. 10. NMR spectra of ^{14}N nuclei in $Mn_3Cu_{0.6}Ge_{0.4}N$ at various temperatures. The data were collected at the fixed resonance frequency of 19.90 MHz.

C. Results of NMR measurements of $Mn_3Cu_{0.6}Ge_{0.4}N$

In this section we discuss the results of ^{14}N-NMR measurements on $Mn_3Cu_{0.6}Ge_{0.4}N$ and exclude the case (2): the magnetic structure is represented by a linear combination of Γ^{5g} and Γ^{4g} antiferromagnetic structures, and the weight of the Γ^{5g} component gradually increases with decreasing T. We then demonstrate the validity of case (3): the Γ^{4g} component is basically absent in the whole temperature regions and the Γ^{5g} antiferromagnetic ordered moment gradually increases with decreasing T.

As shown in Sec. III A the Γ^{4g} ordered moments broadens the ^{14}N-NMR spectrum with a FWHM of 0.23 T/μ_B. On the other hand, the hyperfine fields induced by the Γ^{5g} antiferromagnetic moments is perfectly cancelled out and do not broaden the ^{14}N-NMR spectrum. Thus the presence or absence of the Γ^{4g} component can be judged from the ^{14}N-NMR spectrum.

Figure 10 shows the ^{14}N-NMR spectra of $Mn_3Cu_{0.6}Ge_{0.4}N$ at various temperatures. The data are collected above 200 K because the increase in the linear thermal expansion $\Delta L/L$ is observed from 300 to 200 K. Below 200 K weak ferromagnetism is observed in the magnetic susceptibility.[6] It may complicate the analysis of the NMR spectra. Below T_N the spectrum gradually broadens without a noticeable structure with decreasing T. If we assume case (2), the T dependence of the Γ^{4g} antiferromagnetic moment should follow the result in Fig. 8(a). Then the NMR spectrum should sharpen below the peak temperature of the Γ^{4g} antiferromagnetic moment. Obviously such behavior is not observed in the experimental spectra shown in Fig. 10. This qualitative discussion already invalidates the case (2).

In order to estimate the width induced by the Mn moment we measured the magnetic field dependence of the spectrum

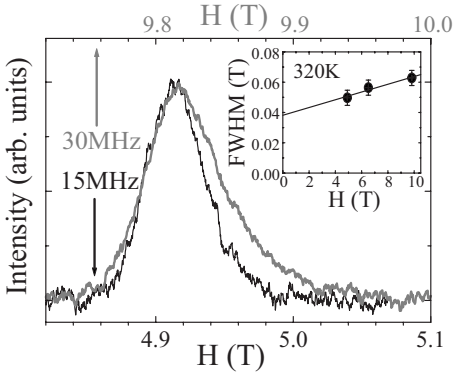

FIG. 11. Main panel: ^{14}N-NMR spectra at the resonance frequencies of 15 and 30 MHz are shown by black and gray lines, respectively. The spectra are obtained at 320 K. Inset: magnetic field dependence of FWHM of ^{14}N-NMR spectra obtained at 320 K. The line shows the fitting to a linear relation.

at 320 K, where the system is in the paramagnetic phase. The ^{14}N-NMR spectra at the resonance frequencies of 15 MHz and 30 MHz are shown in the main panel of Fig. 11. The field dependence of FWHM of the spectrum is shown in the inset. The contribution to the FWHM from the magnetic hyperfine interaction is proportional to the magnetic field in the paramagnetic phase while the quadrupole contribution is independent of field. Then the two contributions can be separated by fitting the field dependence of the FWHM to a straight line as shown in the inset of Fig. 11. The quadrupole contribution to the FWHM is determined to be 0.038 T. Assuming that this is independent of T, the T dependent of the magnetic FWHM is obtained by subtracting the quadrupole contribution from the observed FWHM, as plotted in the main panel of Fig. 12.

The magnetic FWHM increases continuously with decreasing T. The T dependence of $M_{\Gamma^{4g}}$, the amplitude of the Γ^{4g} antiferromagnetic ordered moment, has been determined by neutron diffraction for the case (2) as shown in Fig. 8(a). However, it should be noted that the T_N of $Mn_3Cu_{0.6}Ge_{0.4}N$

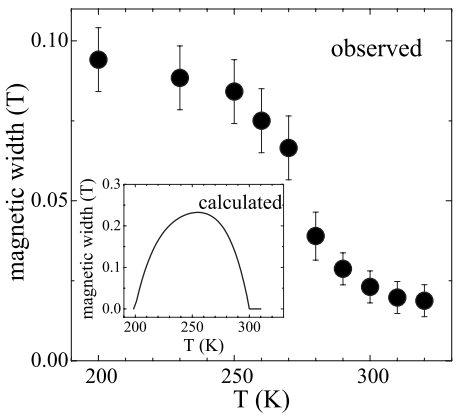

FIG. 12. Main panel: temperature dependence of the magnetic component of FWHM of ^{14}N-NMR spectra with $Mn_3Cu_{0.6}Ge_{0.4}N$. Inset: calculated magnetic FWHM of ^{14}N-NMR spectra of $Mn_3Cu_{0.6}Ge_{0.4}N$ from the Γ^{4g} antiferromagnetic moment is included (see text).

(x=0.4) used in the NMR measurement is about 290 K, which is lower than the $T_N \sim 370$ K of $Mn_3Cu_{0.5}Ge_{0.5}N$ (x =0.5).[6] In order to estimate the value of $M_{\Gamma^{4g}}$ for x=0.4, we assumed that both samples have identical dependence on the reduced temperature T/T_N. The inset of Fig. 12 shows the magnetic FWHM thus calculated from Eq. (6) with the value $A_{\Gamma^{4g}}$=0.23 T. The calculated FWHM has a maximum value of 0.25 T at 250 K, which is three times larger than the FWHM observed at the same temperature. The serious disagreement between the calculated and observed FWHM leads us to conclude that the Γ^{4g} antiferromagnetic component is nearly absent below T_N and that case (2) can also be excluded.

As mentioned in the previous letter, the PDF analysis revealed that the cubic symmetry is locally broken in the present materials.[23] More precisely, the distribution of the Cu/Ge-Mn distance, which has a single peak in the cubic structure, splits into two peaks, indicating rotation of the Mn_6N octahedra. The breaking of the cubic symmetry leads to a finite electric field gradient and allows the Γ^{5g} antiferromagnetic moments to generate a finite hyperfine field. Both of them are forbidden if the system is perfectly cubic. The peak splitting of the Cu/Ge-Mn PDF is almost independent of T in the temperature region where the MVE is observed. Then both the quadrupole contribution to the NMR linewidth and the proportionality constant (hyperfine coupling constant) between the Γ^{5g} antiferromagnetic moment and the linewidth should be independent of temperature in the same T range. These arguments lead us to conclude that the gradual increase in FWHM revealed in the main panel of Fig. 12 must be caused by the gradual increase in the Γ^{5g} antiferromagnetic ordered moment below T_N, which is consistent with the case (3).

The results of neutron scattering and NMR measurements on $Mn_3Cu_{1-x}Ge_xN$ with $x \sim 0.5$ exclude the possibility of the magnetic ordered phase including the Γ^{4g} antiferromagnetic structure. The gradual increase in the Γ^{5g} antiferromagnetic moment causes the broadening of the MVE that provides the gradual increase in linear thermal expansion $\Delta L/L$. The correlation between the amplitude of the magnetic moment and the volume is basically consistent with spin-fluctuation theories.[26] However, the roles of specific magnetic structures have not been considered before. Systematic PDF analysis of $Mn_3Cu_{1-x}Ge_xN$ reveals an increase in the rotation angle of the Mn_6N octahedra with increasing x.[23] This local structural distortion should modify the band structure. Furthermore, the substitution of Ge for Cu will change the number of valence electrons. These two effects change the electronic state, which then changes the magnetic transition from first order at x=0.15 to second order at $x \sim 0.5$ with increasing x. For Invar alloy, $Fe_{64}Ni_{36}$, Curie temperature and the temperature region of low thermal expansion of the mechanical stressed sample, are noticeably larger than the values of the standard sample.[27] A more disordered local environment around Fe atoms relative to the standard sample, the increase in Fe-Fe atomic distance is observed in the mechanical stressed sample.[28] Such local lattice distortion may change the electronic state and the temperature range of the Invar effect also in Invar alloy. Further experiments which directly probe the change in electronic states are still necessary.

Finally, we mention a possible reason why a Γ^{4g} antiferromagnetic component seems to exist in $Mn_3Cu_{0.5}Ge_{0.5}N$, as shown in Fig. 8. As mentioned in Ref. 22, Γ^{5g} and Γ^{4g} antiferromagnetic structures give the largest magnetic scattering intensity to 100 and 110 reflections, respectively. However, the 110 reflection also has the largest contribution from nuclear reflection, as shown in Fig. 7. X-ray absorption fine structure measurement of $Mn_3Cu_{0.7}Ge_{0.3}N$ reveals an increase in the Ge-Mn atomic distance $\sim$0.01 Å around T_N.[29] This atomic shift corresponds to about 0.4% of the Ge-Mn atomic distance. This leads to the speculation that the slight atomic shift causes a small increase in the nuclear Bragg intensity of the 110 reflection. It is likely that this intensity increase has been ascribed to the magnetic scattering of the Γ^{4g} antiferromagnetic structure in our analysis.

IV. CONCLUSION

We have investigated the magnetic structure in $Mn_3Cu_{1-x}Ge_xN$ for $x \sim 0.5$ in detail, in particular, the possible coexistence or competition between the Γ^{5g} and Γ^{4g} antiferromagnetic components near the transition temperature in order to identify the mechanism of the giant negative thermal expansion coefficient. The results of neutron scattering and NMR measurements of $Mn_3Cu_{1-x}Ge_xN$ with $x \sim 0.5$ and the reference material, Mn_3NiN, indicate that, in $Mn_3Cu_{1-x}Ge_xN$ ($x \sim 0.5$), the Γ^{4g} antiferromagnetic component is nearly absent and that the Γ^{5g} antiferromagnetic ordered moment gradually increases with decreasing T. That gradual increase in the Γ^{5g} antiferromagnetic ordered moment causes a gradual increase in the volume (linear thermal expansion), thus resulting in the large negative thermal expansion coefficient of this material.

ACKNOWLEDGMENTS

The authors would like to thank N. Igawa and M. Matsuda for their help with the neutron diffraction measurements, and also M. Yoshida for the magnetic susceptibility NMR sample measurements. This work was performed within a NIMS-RIKEN-JAEA Cooperative Research Program on Quantum Beam Science and Technology. It was supported by a Grant-in-Aid for Scientific Research from the Ministry of Education, Culture, Sports, Science and Technology of Japan and partially by NEDO, Japan.

*Present address: Graduate School of Life Science and Systems Engineering, Kyushu Institute of Technology, Kitakyushu, Fukuoka 808-0196, Japan.

[1] E. F. Wasserman, in *Ferromagnetic Materials*, edited by K. H. J. Buschow and E. P. Wohlfarth (Elsevier, Amsterdam, 1990), Vol. 5.
[2] Y. Kakehashi, Physica B **161**, 143 (1989).
[3] P. Mohn, K. Schwarz, and D. Wagner, Phys. Rev. B **43**, 3318 (1991).
[4] Y. Takahashi and H. Nakano, J. Phys.: Condens. Matter **18**, 521 (2006).
[5] K. Takenaka and H. Takagi, Appl. Phys. Lett. **87**, 261902 (2005).
[6] K. Takenaka and H. Takagi, Mater. Trans. **47**, 471 (2006).
[7] K. Takenaka, K. Asano, M. Misawa, and H. Takagi, Appl. Phys. Lett. **92**, 011927 (2008).
[8] K. Takenaka and H. Takagi, Appl. Phys. Lett. **94**, 131904 (2009).
[9] D. Fruchart and E. F. Bertaut, J. Phys. Soc. Jpn. **44**, 781 (1978).
[10] T. Kaneko, T. Kanomata, and K. Shirakawa, J. Phys. Soc. Jpn. **56**, 4047 (1987).
[11] J.-P. Jardin and J. Labbe, J. Solid State Chem. **46**, 275 (1983).
[12] K. Motizuki and H. Nagai, J. Phys. C **21**, 5251 (1988).
[13] J. P. Bouchaud, Ann. Chim. **3**, 81 (1968).
[14] K. Kamishima, T. Goto, H. Nakagawa, N. Miura, M. Ohashi, N. Mori, T. Sasaki, and T. Kanomata, Phys. Rev. B **63**, 024426 (2000).
[15] E. O. Chi, W. S. Kim, and N. H. Hur, Solid State Commun. **120**, 307 (2001).
[16] M. S. Miao, A. Herwadkar, and W. R. L. Lambrecht, Phys. Rev. B **72**, 033204 (2005).
[17] Ph. l'Heritier, D. Boursier, R. Fruchart, and D. Fruchart, Mater. Res. Bull. **14**, 1203 (1979).
[18] R. Fruchart, R. Madar, M. Barberon, D. Fruchart, and M. G. Lorthioir, J. Phys. (Paris) **32**, 982 (1971).
[19] D. Fruchart, E. F. Bertaut, R. Madar, G. Lorthioir, and R. Fruchart, Solid State Commun. **9**, 1793 (1971).
[20] W. S. Kim, E. O. Chi, J. C. Kim, N. H. Hur, K. W. Lee, and Y. N. Choi, Phys. Rev. B **68**, 172402 (2003).
[21] A. W. Sleight, Inorg. Chem. **37**, 2854 (1998).
[22] S. Iikubo, K. Kodama, K. Takenaka, H. Takagi, and S. Shamoto, Phys. Rev. B **77**, 020409(R) (2008).
[23] S. Iikubo, K. Kodama, K. Takenaka, H. Takagi, M. Takigawa, and S. Shamoto, Phys. Rev. Lett. **101**, 205901 (2008).
[24] K. Takenaka *et al.* (unpublished).
[25] P. J. Brown, in *International Tables for Crystallography*, edited by A. J. C. Wilson (Kluwer Academic, Dordrecht, 1992), Vol. C, Chap. 4.
[26] T. Moriya and K. Usami, Solid State Commun. **34**, 95 (1980).
[27] P. Gorria, D. Martínez-Blanco, M. J. Pérez, J. A. Blanco, A. Hernando, M. A. Laguna-Marco, D. Haskel, N. Souza-Neto, R. I. Smith, W. G. Marshall, G. Garbarino, M. Mezouar, A. Fernández-Martínez, J. Chaboy, L. Fernandez Barquín, J. A. Rodriguez Castrillón, M. Moldovan, J. I. García Alonso, J. Zhang, A. Llobet, and J. S. Jiang, Phys. Rev. B **80**, 064421 (2009).
[28] P. Gorria, R. Boada, A. Fernández-Martínez, G. Garbarino, R. I. Smith, J. Chaboy, J. I. García Alonso, D. Martínez-Blanco, G. R. Castro, M. Mezouar, A. Hernando, and J. A. Blanco, Phys. Status Solidi (RRL) **3**, 115 (2009).
[29] T. Matsuno, K. Takenaka, H. Takagi, D. Matsumura, Y. Nishihata, and J. Mizuki, Appl. Phys. Lett. **94**, 181904 (2009).